Mass distribution and mass-resolved angular distribution in the $^{16}O + ^{238}U$ reaction at sub-barrier energy

T. N. Nag,[1] R. Tripathi,[1,*] S. Sodaye,[1] K. Sudarshan,[1] K. Ramachandran,[2] B. K. Nayak,[2] and P. K. Pujari[1]
[1]*Radiochemistry Division, Bhabha Atomic Research Centre, Mumbai 400085, India*
[2]*Nuclear Physics Division, Bhabha Atomic Research Centre, Mumbai 400085, India*
(Received 8 May 2017; revised manuscript received 1 August 2017; published 11 October 2017)

Background: The angular distribution of fission fragments or products is a sensitive probe to investigate non-compound-nucleus (NCN) fission. However, the gross angular distribution cannot distinguish between different NCN fission processes. Both preequilibrium fission and quasifission contribute to NCN fission and would both result in deviations from the statistical saddle point model (SSPM). Mass-resolved angular distributions of the fission product offers the possibility to distinguish between the two mechanisms [Sodaye *et al.*, Phys. Rev. C **95**, 014612 (2017); Tripathi *et al.*, *ibid.* **88**, 024603 (2013); Vorkapic and Ivanisevic, *ibid.* **55**, 2711 (1997)].
Purpose: Mass and mass-resolved angular distributions of fission products have been measured in the $^{16}O + ^{238}U$ reaction at $E_{lab} = 85.3$ MeV to investigate the dominant NCN fission mechanism at sub-barrier energy.
Method: Mass and mass-resolved angular distributions were measured by recoil catcher technique followed by offline γ-ray spectrometry.
Results: The mass distribution was observed to be predominantly asymmetric. The angular anisotropy of the fission products was observed to be independent of their mass.
Conclusions: The mass independence of the angular anisotropy suggested quasifission to be the dominant NCN fission process. This was further confirmed from the underestimation of angular anisotropy by theoretical calculations even after including the contribution from preequilibrium fission.

DOI: 10.1103/PhysRevC.96.044608

I. INTRODUCTION

Investigation of non-compound-nucleus (NCN) fission processes in reaction systems with low entrance channel Coulomb repulsion has been actively pursued in recent past [1–7]. Measurements of mass distribution [3] have shown onset of NCN fission in the preactinide region around $Z_P Z_T \sim 1000$, where Z_P and Z_T are the proton numbers of the projectile and the target respectively. Measurement of evaporation residue cross sections in the $^{28}Si + ^{176}Yb(Z_P Z_T = 980)$ reaction showed fusion suppression at near barrier energies [2]. These observations suggest that the onset of NCN fission in the actinide region should be further reduced as fission barriers are lower and saddle point configurations are more compact compared to those in the preactinide region. At low beam energies, where maximum angular momentum (l_{max}) is lower compared to the critical value at which fission barrier vanishes, two types of NCN fission processes, namely, preequilibrium fission [8,9] and quasifission [10], are observed. The preequilibrium fission model was proposed to explain the anomalous fission fragment angular distribution [8,9] based on the incomplete equilibration of the K degree of freedom, where K is the projection of the angular momentum vector on the nuclear symmetry axis. Based on this model, the contribution from preequilibrium fission would be present if entrance channel mass asymmetry (α) of a reaction system is lower than the Businaro-Gallone critical mass asymmetry (α_{BG}). Thomas *et al.* [11] suggested that the contribution from preequilibrium fission would be present even in reaction systems with $\alpha > \alpha_{BG}$ in the case of deformed actinide targets, due to the initiation of the fusion process at internuclear separation larger than the location of the fusion barrier corresponding to a spherical projectile-target combination. The magnitude of the contribution from preequilibrium fission depends on the ratio of the fission barrier to the temperature of the fissioning nucleus at the saddle point. On the other hand, in the case of quasifission, the fissioning system escapes into an exit channel without being captured inside the saddle point. Here again, as fission occurs without complete K equilibration, the fission fragment angular distribution is anomalous. In addition, there is a suppression in the formation cross section of the evaporation residues compared to the prediction of statistical model, and a broadening of the mass distribution is expected. Hinde *et al.* [12] measured the fission fragment angular distribution in the $^{16}O + ^{238}U$ reaction at near-barrier and sub-barrier energies. These studies showed a sharp increase in the angular anisotropy as beam energy decreased through the entrance channel Coulomb barrier. This observation was attributed to the contribution from an orientation dependent quasifission. In the case of contribution from quasifission, the evaporation residue cross section, though extremely low in the heavy actinide region, should be further suppressed. However, Nishio *et al.* did not observe any fusion suppression in this reaction based on a measurement of the evaporation residue cross section [13]. It was proposed that the anomalous fission fragment angular distribution may be due to the contribution from preequilibrium fission. Measurement of the mass distribution in this reaction by Banerjee *et al.* [14] showed a broadening in the mass distribution at sub-barrier energies which was attributed to the contribution from quasifission. However, measurement of the mass distribution by Yanez *et al.*

*Corresponding author: rahult@barc.gov.in

[15] showed lower variance than that observed by Banerjee *et al.* [14]. Vorkapic and Ivanisevic [16] attributed the mass dependent anisotropy in the $^{16}O + ^{232}Th$ reaction [17] to the variation of fission time scale with varying asymmetry of mass division, and thus a difference in the magnitude of the preequilibrium fission contribution. Based on the liquid drop model, the fission time scale would be the lowest for symmetric division, thus leading to maximum angular anisotropy. Recent measurements on the mass-resolved angular distribution in $^{20}Ne + ^{232}Th$ [18] and $^{28}Si + ^{232}Th$ [19] reactions showed similar results. In the case of quasifission, where the fissioning system does not encounter a fission barrier on its way to fission, such a dependence is expected to be absent. In fact for reaction systems with lower entrance channel mass asymmetry, where the fission fragment mass distribution is broader due to incomplete mass equilibration, the anomaly would be expected to be more pronounced for asymmetric products [20]. This would be due to the formation of asymmetric products at a shorter time scale, as the fissioning system is not reaching inside the unconditional saddle point. Thus, the mass dependence of the anisotropy offers a possibility to distinguish between the contribution from preequilibrium fission and quasifission as the gross fission fragment angular distribution would be anomalous in both the cases. It is important to carry out measurements on the mass-resolved angular distribution at sub-barrier energy as quasifission is likely to dominate at these beam energies, with a pronounced difference in angular anisotropies for CN and NCN fission.

In the present work, mass and mass-resolved angular distributions have been measured in the $^{16}O + ^{238}U$ reaction at an average beam energy (E_{lab}) of 85.3 MeV, corresponding to an E_{cm}/V_c value of 0.95, to investigate the dominant NCN fission process in this reaction at sub-barrier energy.

II. EXPERIMENTAL DETAILS

Measurements were carried out with an 87 MeV ^{16}O beam from the BARC-TIFR Pelletron-LINAC facility in Mumbai. A self-supporting target of ^{nat}U having a thickness of 3 mg/cm^2 was mounted at 45° with respect to the beam at the entry of a half-cylindrical chamber having a diameter 55.4 mm and a length of 90.0 mm. Energy loss of the beam in the target, calculated using the code SRIM [21], was 6.3 MeV. The fusion cross section weighted average beam energy in the target was 85.3 MeV, which will subsequently be referred to as E_{lab}. The fusion cross section was calculated using the couple channel code CCFUS [22] with the deformation data of the excited states of the projectile and target taken from Ref. [23]. For the measurement of mass distribution, a super pure Al catcher foil of thickness 6.75 mg/cm^2 was placed after the target downstream to collect fission products recoiling out of the target in the forward hemisphere. After irradiation of about ∼10 h, the catcher foil was removed and assayed for γ-ray activity of the fission products. For measurement of angular distribution, Al foils of thickness 6.75 mg/cm^2 were mounted at the inner wall of the cylindrical chamber to collect the fission products recoiling out of the target in the angular range from 90° to nearly 0°. Irradiation was carried out for about 48 h. After irradiation, the foils were removed and cut into six stripes corresponding to different angles, and were assayed for γ-ray activity of the fission products. For both mass distribution and mass-resolved angular distribution, the same target was used to keep the beam energy identical in both the cases.

The γ-ray activity of the fission products was assayed using precalibrated high-purity germanium (HPGe) detectors. Decay of the fission products was followed for about two months. Fission products were unambiguously identified by matching their half-lives and characteristic γ-ray energies. In addition to fission products, γ rays of the products formed in onenucleon transfer/pickup were also observed. Decay data of radionuclides used in the present work is given in Table I [24,25]. From the γ-ray spectra, areas under the characteristic γ-ray peaks of the fission products were obtained using the peak area analysis software PHAST [26]. The peak areas were used to obtain yields of different fission products. Details about the determination of yields can be found in Ref [18]. Yields of different fission products and a few transfer products are also given in Table I. Experimentally measured yields of the fission products are either cumulative (C) or independent (I) as mentioned in the table. Experimental yields of fission products and evaporation residues were normalized with respect to the total fission yield obtained by integrating the fitted mass distribution. Fitting of the mass distribution is discussed in the next section.

III. RESULTS AND DISCUSSION

A. Mass distribution

In order to obtain mass distribution, yields of the fission products in the forward catcher foil were corrected for the charge distribution. With the approximation that the fission products emitted in both forward and backward hemispheres are equally stopped in the target, the average retention factor for the target was about ∼10%. The yield of a mass chain $Y(A)$ is obtained from experimentally measured independent yield IN(A,Z) or cumulative yield CU(A,Z) of a fission product with mass A and atomic number Z, using the following equations:

$$Y(A) = \mathrm{IN}(A,Z)/\mathrm{FIY}(A,Z), \tag{1}$$

$$Y(A) = \mathrm{CU}(A,Z)/\mathrm{FCY}(A,Z), \tag{2}$$

where FIY(A,Z) and FCY(A,Z) are fractional independent and cumulative yields respectively and are calculated using the equations

$$\mathrm{FIY}(A,Z) = \frac{1}{\sqrt{2\pi\sigma_z^2}} \int_{Z-0.5}^{Z+0.5} e^{-(Z-Z_p)^2/2\sigma_z^2} dZ, \tag{3}$$

$$\mathrm{FCY}(A,Z) = \frac{1}{\sqrt{2\pi\sigma_z^2}} \int_{-\infty}^{Z+0.5} e^{-(Z-Z_p)^2/2\sigma_z^2} dZ. \tag{4}$$

Thus, charge distribution correction requires Z_P (most probable charge for a given mass chain) and σ_Z (width of the isobaric yield distribution) [27]. It has been observed in several studies that the σ_Z value does not vary significantly in a moderate excitation energy range or with small variation in the projectile-target combination. In the present work, the

TABLE I. Decay data [24,25] and yields of fission and transfer products in the $^{16}O + ^{238}U$ reaction at a beam energy of 85.3 MeV ($E_{c.m.}/V_c = 0.95$). Measured yields of the fission products are either cumulative (C) or independent (I) as mentioned in the table. Calculated fractional independent yield (FIY) or fractional cumulative yield (FCY) are also given in the table.

Nuclide	Half-life	E_γ (keV)	Intensity (%)	Yield (%)	FIY or FCY
$^{85}Kr^m$	4.48 h	151.2	75	0.47 ± 0.31 (C)	0.994
^{88}Kr	2.83 h	196.6	25.9	1.22 ± 0.39 (C)	0.854
^{91}Sr	9.63 h	1024.3	33.4	1.45 ± 0.89 (C)	0.979
^{92}Sr	2.71 h	1383.9	90	1.29 ± 0.43 (C)	0.937
92Y	3.54 h	934.5	13.9	2.6 ± 1.5 (C)	0.997
^{95}Zr	64.02 d	756.7	55.4	1.98 ± 0.36 (C)	0.994
^{97}Zr	16.74 h	743.4	92.6	2.14 ± 0.37 (C)	0.933
^{99}Mo	2.75 d	140.5	90.7	2.90 ± 0.15 (C)	0.998
^{103}Ru	39.25 d	497.1	89.5	3.21 ± 0.19 (C)	1.0
^{105}Ru	4.44 h	724.2	46.7	3.1 ± 0.93 (C)	0.993
^{105}Rh	35.36 h	318.9	19.2	3.6 ± 0.7 (C)	1.0
^{105}Rh	35.36 h	306.1	5.13	4.0 ± 2.9 (C)	1.0
$^{111}Pd^m$	5.5 h	172.2	33.5	0.70 ± 0.40 (C)	0.228
^{112}Pd	21.05 h	617.4	50	2.45 ± 0.56 (C)	0.919
$^{113}Ag^g$	5.37 h	298.6	10	2.9 ± 1.4 (C)	0.984
$^{115}Cd^g$	2.23 d	336.2	49.7	2.3 ± 0.41 (C)	0.991
$^{115}In^m$	4.49 h	336.2	45.8	1.7 ± 0.61 (C)	1.0
$^{117}Cd^m$	3.36 h	158.6	109	1.92 ± 0.38 (C)	0.914
$^{117}Cd^m$	3.36 h	552.9	125	1.45 ± 0.26 (C)	0.914
^{122}Sb	2.72 d	564	70.8	0.43 ± 0.22 (I)	0.086
$^{124}Sb^g$	60.2 d	602.7	98.4	1.13 ± 0.10 (I)	0.316
$^{126}Sb^g$	12.46 d	414.8	83.2	0.75 ± 0.09 (I)	0.467
^{127}Sb	3.85 d	473	24.7	1.2 ± 0.5 (C)	0.520
^{128}Sb	9.01 h	754	100	0.35 ± 0.3 (C)	–[b]
$^{130}I^g$	12.36 h	536.1	99	1.08 ± 0.31 (I)	0.435
^{131}I	8.02 d	364.5	81.7	2.75 ± 0.85 (C)	0.700
$^{133}I^g$	20.8 h	529.9	87	1.85 ± 0.78 (C)	–[b]
^{134}I	52.5 m	884	64.9	1.7 ± 0.92 (C)	–[b]
^{140}Ba	12.75 d	537.3	24.4	1.8 ± 0.40 (C)	–[b]
^{140}La	1.68 d	487	45.5	0.75 ± 0.50 (C)	0.833
^{140}La	1.68 d	815.8	23.2	1.8 ± 0.65 (C)	0.833
^{142}La	91.1 m	641.2	47.4	1.1 ± 0.7 (C)	–[b]
^{143}Ce	33.02 h	293.27	42.8	2.05 ± 0.49 (C)	0.757
^{238}Np[a]	2.12 d	984.5	27.8	0.048 ± 0.006	
^{239}Np[a]	2.36 d	277.6	14.5	0.21 ± 0.01	
^{237}U[a]	6.75 d	208	21.7	0.49 ± 0.04	

[a]Yields are reported relative to fission.

[b]Yields not included in mass distribution as $A/Z \geqslant 2.491$.

σ_Z value of 0.80, obtained from our earlier measurement in the $^{20}Ne + ^{232}Th$ [18] reaction was used. The Z_P value for a mass chain with mass number A was calculated as $A/[(A_{CN} - \nu_T)/Z_{CN}]$, where A_{CN} and Z_{CN} are, respectively, the mass number and proton number of the compound nucleus, and ν_T is the average number of neutrons emitted per fission. The value of ν_T was calculated using the prescription of Kozulin *et al.* [28]. Fractional independent or cumulative yields calculated using Eqs. (3) and (4) respectively (given in Table I) were used to correct the yields of the fission products to obtain the mass yields, which are plotted in Fig. 1. Filled circles are experimental points and open circles are the mass yields assigned to the complimentary masses calculated as $(A_{CN} - \nu_T - A)$, where A is the fission product mass for which the yield has been measured experimentally. It can be seen from the figure that the mass distribution is predominantly asymmetric. Yields of a few Sb isotopes in the symmetric region are outliers. This may be due to the inadequacy of the charge distribution parameters in correcting the independent yields, as the magnitude of correction is very large. For example, the correction factor (1/FIY) for ^{122}Sb is about ∼11.6 and for ^{124}Sb it is about ∼3.2. However, experimental yields of most of the fission products are cumulative and include the yields of the preceding members of the respective isobaric chain. Thus, the charge distribution correction is not very significant for most of the fission products with cumulative yields. Therefore, uncertainties in the charge distribution would not affect the nature of the mass distribution. The observed asymmetry cannot be attributed to the contribution from transfer induced fission as it is expected to be small

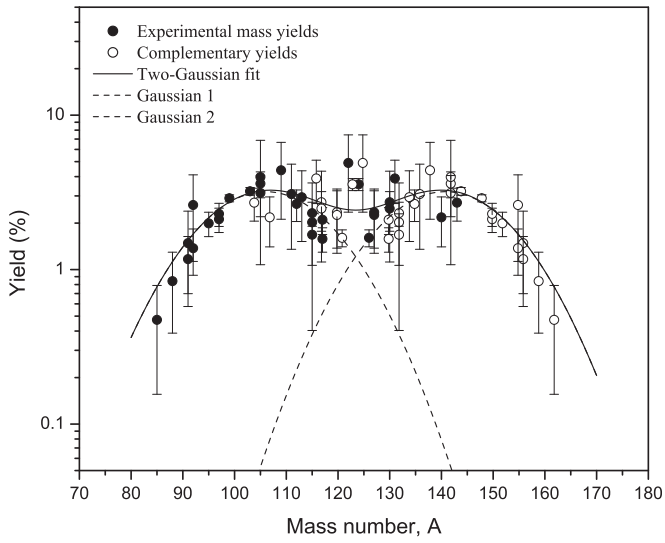

FIG. 1. Mass distribution in the $^{16}O + ^{238}U$ reaction at $E_{lab} = 85.3$ MeV ($E_{c.m.}/V_c = 0.95$).

at sub-barrier and near-barrier energies. Using folding angle data for the $^{16}O + ^{238}U$ reaction in Ref. [12], the contribution from transfer induced fission can be estimated to be around ∼30% at $E_{lab} = 83$ MeV, which is slightly lower than the beam energy of the present study. As the complete fusion cross section would sharply increase with increasing beam energy, the contribution from transfer induced fission would be lower in the present study than that in Ref. [12]. In Ref. [29], the contribution from transfer induced fission has been reported to be <1% in $^{16}O + ^{232}Th$, $^{12}C + ^{236}U$, and $^{11}B + ^{237}Np$ reactions at near barrier energies. Observation of large yields of $^{239}Np(0.21 \pm 0.01)$ and $^{237}U(0.49 \pm 0.04)$, relative to the fission, formed in one-nucleon transfer and pickup reactions respectively, also suggested that the contribution from transfer induced fission is small. This is expected as excitation energy of the fissioning nuclei would be low in one-nucleon transfer/pickup reactions. A small yield for ^{238}Np (0.048 ± 0.006; relative to total fission) was also observed. The contribution to transfer induced fission would mainly result from the α transfer channel due to the larger excitation energy and angular momentum of the fissioning nucleus as compared to that in proton/neutron transfer induced fission. The contribution from transfer induced fission was estimated by fitting the lower mass wing of the mass distribution to two components: one arising from full momentum transfer and the other arising from αtransfer. Variance of the mass distribution for the α transfer induced fission was taken from the $^{4}He + ^{238}U$ reaction at $E_{lab} = 24.1$ MeV [30]. The contribution from transfer induced fission was varied manually and the quality of fitting was judged by the error on the contribution from full momentum transfer fission, as the chi-square value did not change significantly with variation in the transfer fission contribution. Based on the decrease in the fitting error on the full momentum transfer fission contribution, the contribution from transfer induced fission was estimated to be in the range of ∼7–15%. While fitting the overall mass distribution, as was done in our earlier studies [18,19], the fission products with $A/Z \geqslant 2.491$ were not included in the mass distribution as these products may have a larger contribution from TF even though the magnitude of overall transfer induced fission may be small. In the measurements carried out by Yanez *et al.* [15] and Banerjee *et al.* [14], the mass distribution was reported to be symmetric at similar beam energy. It should be mentioned here that the experimental mass distribution in the present work would more likely be an admixture of both symmetric and asymmetric fission owing to the large variation of the beam energy in the target from 87 to 80.7 MeV due to the energy degradation. An attempt to fit the experimental mass distribution as a mixture of symmetric and asymmetric fission gave variance values which had more than 50% fitting error, as it was difficult to fix the relative contribution from the two types of fission. Therefore, the mass distribution was fitted to a sum of two Gaussian functions, assuming it to be predominantly asymmetric. The fitting was performed with four free parameters: (i) area of the Gaussian curve (assumed to be same for both the components), (ii) widths of the two Gaussian curves, and (iii) centroid of the lower peak in the mass distribution. The mass of the fissioning system was fixed as 247 based on the ν_T value of 7.2 as calculated using the prescription of Kozulin *et al.* [28]. Fitted curves are shown in Fig. 1. Dashed curves represent individually fitted Gaussian functions and the solid curve is their sum, which describes the experimental mass distribution reasonably well. This observation suggests that some amount of asymmetric fission may be present in this reaction system in the other studies also [14,15], though it is not visible due to the dominant symmetric component. Further, the finite mass resolution of the online measurements may also contribute to smearing of asymmetry in the mass distribution. However, in the present work the situation is reversed as beam energy extends to the deep sub-barrier energy. Recently, Leguillon *et al.* [31] measured the fission fragment mass distributions for several Th, Pa, and U isotopes through multinucleon transfer with well defined excitation energies. These studies show that asymmetric fission remains dominant up to an excitation energy of 40 MeV, though the relative contribution from symmetric and asymmetric component varies with neutron and proton numbers of fissioning nucleus. The compound nucleus in the present study is heavier than those in Ref. [31]; however, the mass distribution is expected to be qualitatively similar to those observed in Ref. [31], as the average excitation energy in the present study (E^*) is 41.6 MeV.

B. Mass-resolved angular distribution

Angular distributions of the fission products in the laboratory frame of reference were obtained by dividing their yields in different catcher foils with the solid angle of the respective catcher foils, $(\cos\theta_1 - \cos\theta_2)$, where θ_1 and θ_2 are the laboratory angles corresponding to the two edges of the strip. The details can be found in Ref. [18]. The laboratory angular distributions of the fission products were transformed into the center-of-mass (c.m.) frame of reference using the standard kinematic equations, with kinetic energies calculated using the prescription of Rossner *et al.* [32]. The center-of-mass (c.m.) angular distributions $W(\theta_{c.m.})$ versus $\cos^2(\theta_{c.m.})$ for various fission products formed in the $^{16}O + ^{238}U$ reaction

are shown in Fig. 2. Angular distributions of the fission products with $A/Z \geqslant 2.491$ are shown as open circles. The plot of $W(\theta_{\mathrm{c.m.}})$ versus $\cos^2(\theta_{\mathrm{c.m.}})$ was fitted by a linear function $W(\theta_{\mathrm{c.m.}}) = a + b\cos^2(\theta_{\mathrm{c.m.}})$, and the anisotropy $W(0)/W(90)$ was obtained as $1 + b/a$. The plot of anisotropy values as a function of fission product mass is shown in Fig. 3. It can be seen from the figure that the experimental anisotropies are independent of the fission product mass. This observation is different from that in earlier studies at above barrier energies [16–19], which showed an increase in the angular anisotropy in the symmetric mass region. Higher anisotropy in the symmetric mass region was attributed to the lesser degree of K equilibration as compared to that in the asymmetric mass division. This is due to the larger barrier for asymmetric mass division as predicted by the liquid drop model (LDM). The absence of mass dependence of anisotropy observed in the present study suggests that the fissioning system is not reaching inside the unconditional saddle point and, therefore, variation in the barrier height is not playing a role in governing the angular anisotropy. The average anisotropy (shown as a solid line in Fig. 3) was obtained as 2.10 ± 0.21. The uncertainty quoted on the average anisotropy is the standard deviation. This value is close to that observed by Hinde *et al.* [12] at similar beam energy and is much higher than that expected for compound nucleus fission. Nishio *et al.* [13] suggested that the anomaly in the angular distribution may be due to the contribution from preequilibrium fission. In order to investigate this aspect, calculations were preformed with and without including the contribution from preequilibrium fission.

For the compound nucleus fission, angular distribution of the fission products can be described by the statistical saddle point model (SSPM), which assumes that the orientation of the fissioning nucleus with respect to the angular momentum vector does not change beyond the saddle point and the two fission fragments separate along the nuclear symmetry axis [33,34]. According to this model, several K states (K being the projection of the angular momentum vector on the nuclear symmetry axis) are populated at the saddle point with a Gaussian distribution characterized by a variance K_0^2. Based on the SSPM, the angular distribution of the fission products for a reaction involving zero projectile-target spin can be given as [33,34]

$$W(\theta_{\mathrm{c.m.}}) \propto \sum_{l=0}^{\infty} \frac{(2l+1)^2 T_l e^{-\frac{(l+1/2)^2 \sin^2\theta_{\mathrm{c.m.}}}{4K_0^2}} J_0\left[i(l+1/2)^2 \sin^2\theta_{\mathrm{c.m.}}/4K_0^2\right]}{\left(2K_0^2\right)\mathrm{erf}\left[(l+1/2)/\left(2K_0^2\right)^{1/2}\right]}, \tag{5}$$

where T_l is the transmission coefficient, J_0 is the zeroth-order Bessel function and "erf" is the error function. ${K_0}^2$ is the variance of the K distribution. The l distribution of the fissioning nucleus was calculated using the coupled channel code CCFUS [22]. The variance K_0^2 was calculated as $I_{\mathrm{eff}}T/\hbar^2$, where I_{eff} is effective moment of inertia and T is temperature of the fission nucleus at the saddle point. I_{eff} is given as $(1/I_{\parallel} - 1/I_{\perp})^{-1}$, where $I_{\parallel}$ and $I_{\perp}$ are moment of inertia values for rotation about the nuclear symmetry axis and about an axis perpendicular to the nuclear symmetry axis, respectively. For a pure LDM potential energy surface there would be one saddle point, whereas for the shell corrected potential energy surface for ^{254}Fm there would be two saddle points, though the energy of the second saddle will be much lower than that of the first [35]. As discussed earlier, the overall mass distribution in the present study is asymmetric. However, the contribution from symmetric fission may also be present. Therefore, the calculations have been performed for the two extreme cases: (i) the fission process is purely governed by the LDM potential energy surface and (ii) the fission process is governed by the shell corrected potential energy surface with the shell correction present in maximum strength. It should be mentioned here that the actual fission process would lie in between these two extremes and the magnitude of shell correction would vary due to multichance fission. For the first case, the LDM potential energy of the fissioning nucleus was calculated for asymmetry values corresponding to different fission fragment masses using the prescription of Brack *et al.* based on a (c,h,α) parametrization [36]. The parameter c defines the elongation of the fissioning nucleus relative to the radius of the spherical ground state (R_0) such that the total elongation of the fissioning nucleus is $2cR_0$. The parameter h is related to the thickness of the neck for a given value of c. The parameter h was chosen in such a way that the $h = 0$ line approximately passes through the bottom of the valley of the LDM potential energy surface of the fissioning nucleus. It should be mentioned here that, even for $h = 0$, shape of the fissioning nucleus would have appreciable neck for larger values of c. The parameter α describes asymmetry of the shape and $\alpha = 0$ corresponds to symmetric shape. In the present LDM calculations, the value of h was taken as zero. Calculations were performed for $l = 0$, which should not significantly affect the outcome of the calculations as the average angular momentum ($\langle l \rangle = 9$) of the fissioning nucleus is low in the present study. The value of c, corresponding to the maximum on the potential energy curve, increased from 1.34 for symmetric mass division to 1.38 for the most asymmetric mass division observed in the present study. The fragment masses were converted into product masses assuming distribution of fission neutrons between the two complimentary fragments in the ratio of the masses of the fragments. The I_{eff} values were calculated using the equation based on (c,h,α) parametrization as given in Ref. [35] and are plotted in Fig. 4(a). A small drop for asymmetric masses is a result of shifting of the maximum towards higher c values. The temperature of the fissioning nucleus was calculated as $T = \sqrt{(E^* - B_f - E_{\mathrm{rot}} - E_v)/(A_f/9)}$, where $E^*(= E_{\mathrm{c.m.}} + Q_{gg})$ is the excitation energy of the compound nucleus. $E_{\mathrm{c.m.}}$ is the projectile energy in the c.m. frame of reference and Q_{gg} is the

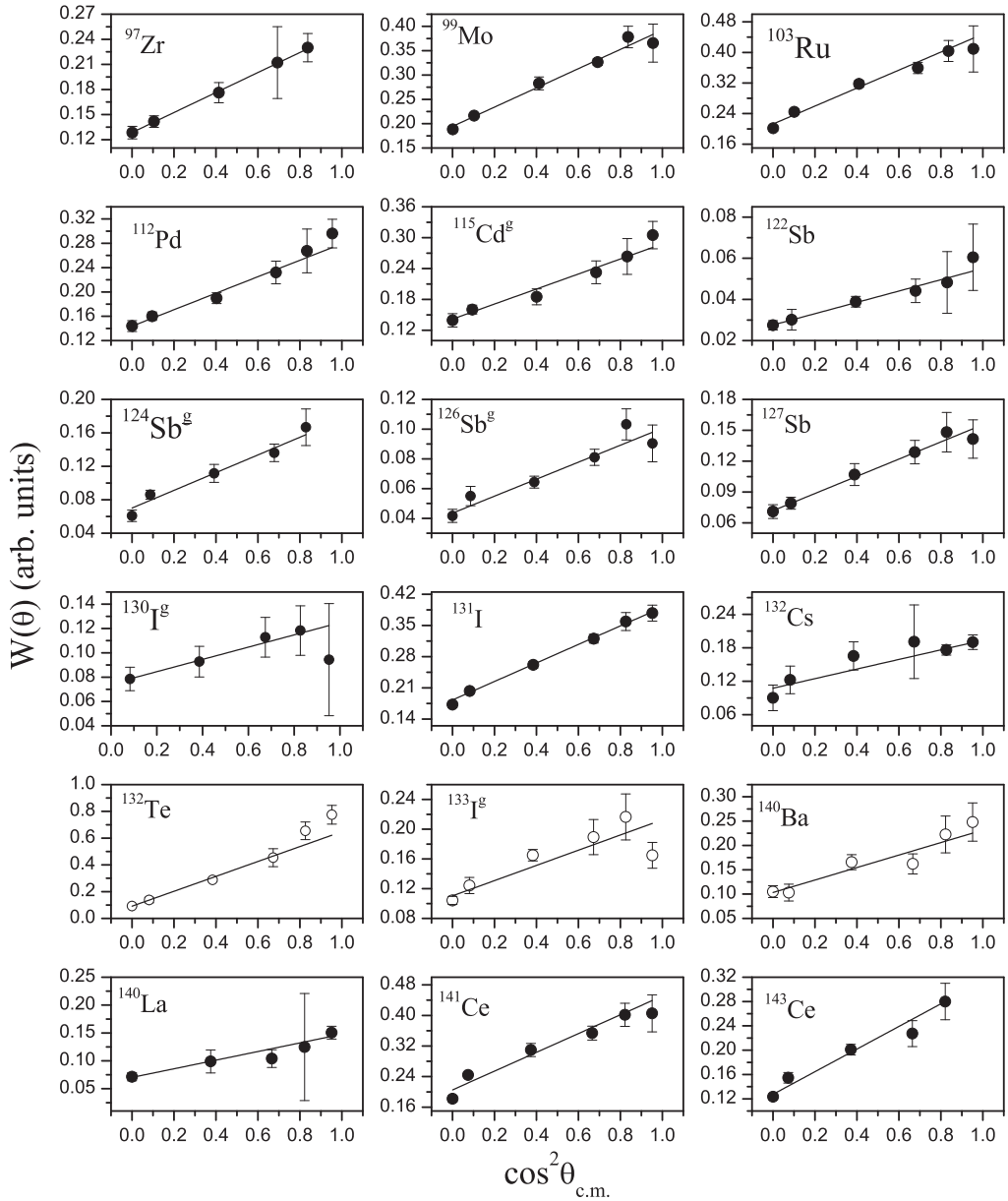

FIG. 2. Plot of angular distributions [$W(\theta_{\text{c.m.}})$ vs $\cos^2(\theta_{\text{c.m.}})$] for different fission products in the $^{16}\text{O} + ^{238}\text{U}$ reaction at $E_{\text{lab}} = 85.3$ MeV ($E_{\text{c.m.}}/V_{\text{c}} = 0.95$). Data for fission products with $A/Z \geqslant 2.491$ are shown by open circles.

ground state Q value for compound nucleus formation. E_{rot} is the rotational energy of the fissioning nucleus at the saddle point and was approximated as $l^2\hbar^2/2I_{\perp}$, and E_{ν} is the energy lost in emission of prefission neutrons. In order to calculate E_{ν}, the number of prefission neutrons were calculated using the prescription of Kozulin *et al.* [28]. In the present calculations, the fissioning nucleus mass was approximated as that of the compound nucleus, as the majority of neutrons are expected to be emitted beyond the saddle point. B_f is the fission barrier, which was taken as the maximum value along the potential energy curve on the fission path corresponding to a given fission product. A plot of the barrier energy or deformation energy for different fission product masses calculated using LDM [36] is shown in Fig. 4(b) as filled circles. Anisotropies calculated using SSPM [33,34], with the assumption of the fission process being purely governed by LDM, are shown as open stars in Fig. 3. It can be seen that the calculated values are nearly constant, though much lower than the experimental anisotropies.

When considering the other extreme that the fission process is governed by the potential energy surface with shell corrections present in maximum strength, it was assumed that the angular distribution is frozen in the vicinity of the second saddle as it would result in the highest possible anisotropy for compound nucleus fission. This was due to the larger elongation of the fissioning nucleus which would result in lower values of I_{eff}. At the second saddle, the fissioning nucleus becomes unstable towards asymmetric deformation. The symmetric and asymmetric modes of fission are approximately characterized by the (c,h) values of (1.6,−0.075)

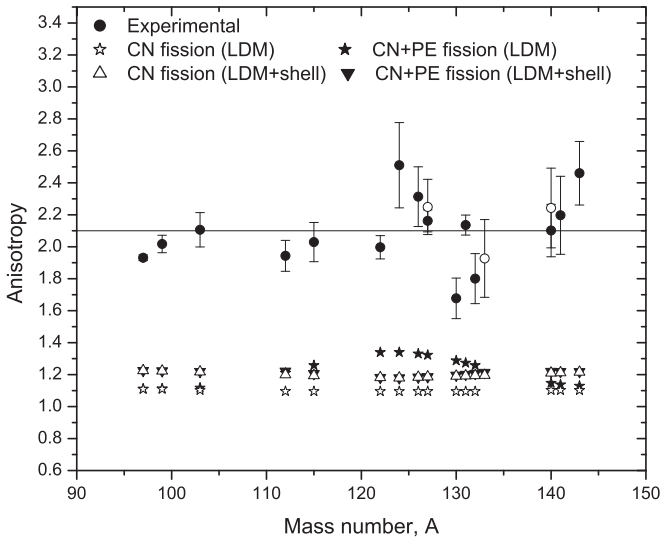

FIG. 3. Plot of angular anisotropy values as a function of fission product mass number. Circles are experimental points. Data for fission products with $A/Z \geqslant 2.491$ are shown by open circles. Open stars and triangles are SSPM [33,34] calculations for compound-nucleus fission. Filled stars and inverted triangles are the anisotropy values calculated after including the contribution from preequilibrium fission (see text for details).

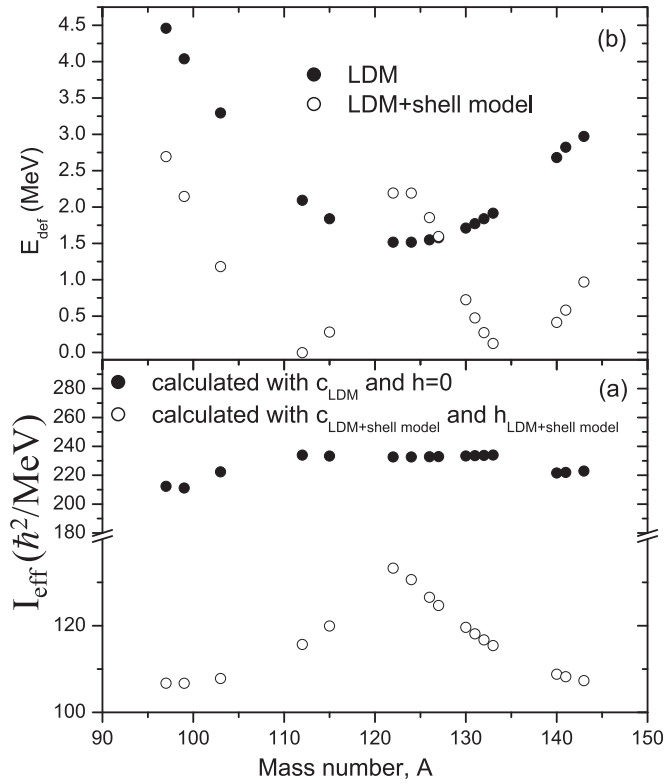

FIG. 4. (a) Moment of inertia of the fissioning nucleus in the vicinity of the liquid drop model saddle point (filled circles) and in the vicinity of the second saddle of the shell corrected potential energy surface (open circles). (b) Deformation (potential) energy of the fissioning nucleus as a function of fission product mass calculated using the liquid drop model (filled circles) and the liquid drop model with shell correction (open circles).

and (1.75,0.027) respectively [37,38]. Using an empirical procedure given in Ref. [37], the shell correction was applied to the LDM potential energy calculated for $c = 1.6$ and $h = 0$. The shell corrected potential energy was calculated as $E_{\rm def}^{\rm LDM} + \delta W_f(M)e^{-\lambda E^*}$, where E^* is the excitation energy of the fissioning nucleus and λ is the shell damping factor. In the present calculations, the term $e^{-\lambda E*}$ was taken as unity as the magnitude of shell correction was assumed to be maximum. The quantity $\delta W_f(M)$ is the shell correction for a particular mass asymmetry leading to a fission fragment with mass M and is given as $\delta W_f(A_f/2)e^{-\gamma(M-A_f/2)}$, where A_f is the mass of the fissioning nucleus. The parameter $\delta W_f(A/2)$ is the shell correction at symmetry. The parameter γ governs the mass dependence of the shell correction and was taken as 0.015 [39]. The $\delta W_f(A/2)$ value of 3.4 MeV reproduced the barriers for symmetric and asymmetric fission modes at the second saddle as given in Ref. [35]. The shell corrected potential energies (relative to the LDM ground state) are shown in Fig. 4(b) as open circles. These values were used for the calculation of the temperature of the fissioning nucleus as well as in the calculation of angular anisotropies including preequilibrium fission, as will be discussed later. In order to calculate $I_{\rm eff}$ for different mass asymmetry values, a continuous linear variation of c and h with mass asymmetry was assumed for the simplicity of the calculations. A plot of $I_{\rm eff}$ values of the fissioning nucleus for different mass asymmetry values in the vicinity of the second saddle is shown in Fig. 4(a) as open circles. The decrease in $I_{\rm eff}$ with increasing mass asymmetry is a result of increasing c value. Angular anisotropies calculated using SSPM [33,34], considering that the fission process is governed by the shell corrected potential energy surface, are shown as open triangles in Fig. 3. These values, though larger than those calculated assuming a pure LDM potential energy surface of the fissioning nucleus, are still much lower compared to the experimental anisotropies.

The large underestimation of the experimental anisotropies by SSPM [33,34] confirms the contribution from the NCN fission. Based on an increase in the anisotropy of the gross fission fragment angular distribution for the $^{16}O + ^{238}U$ reaction at sub-barrier energy, Hinde *et al.* [12] proposed the contribution from an orientation dependent quasifission. According to this model, as the beam energy decreases and approaches the fusion barrier, collision trajectories involving collision of the projectile with the tip of the deformed target nucleus contribute more to the projectile capture. However, as the composite system may be more elongated compared to the unconditional saddle point in this case, it would undergo quasifission. A sharp increase in the angular anisotropy at sub-barrier energy was attributed to an increase in the contribution from such collision trajectories. However, based on the measurement of evaporation residue cross section, Nishio *et al.* did not observe any fusion hindrance in this reaction at sub-barrier energies [13]. In these studies it was proposed that the anomalous fission fragment angular distribution in this reaction may be due to the contribution from preequilibrium fission. In order to investigate this, SSPM [33,34] calculations were performed

with the inclusion of the preequilibrium fission model by coupling the entrance channel K distribution to the saddle point K distribution. Details of the calculations can be found in Refs. [11,18]. According to the preequilibrium fission model, the magnitude of its contribution depends on the ratio of the fission barrier to the temperature of the fissioning nucleus. As was done for compound nucleus fission, calculations including preequilibrium fission were performed for the LDM potential energy surface as well as the shell corrected potential energy surface. While using the shell corrected potential energy, the ground state shell correction from Ref. [35] was added to the barrier energies shown in Fig. 4(b) (open circles). Anisotropies calculated for the pure LDM potential energy surface are shown as filled stars in Fig. 3. As expected, the calculated anisotropy is higher in the symmetric mass region due to lower barrier for symmetric fission. Anisotropies calculated for the shell corrected potential energy surface are shown as filled inverted triangles in Fig. 3. As can be seen from the figure, there is no significant change compared to the compound nucleus fission in this case, as the overall fission barrier is higher (5.3 and 3.1 MeV for symmetric and asymmetric fission modes) after adding the ground state shell correction which results in a larger fission time scale, leading to a broader K distribution. Thus, theoretical calculations highly underestimate the experimental anisotropies even after including the contribution from preequilibrium fission. This observation further confirms that the anomaly in the angular distribution at the sub-barrier energy in the present study is more likely due to the contribution from quasifission, where fission is occurring at a shorter time scale with narrower K distribution as compared to that expected in the case of preequilibrium fission. The absence of suppression in the evaporation residue cross section [13] indicates the complex nature of the equilibration process in various degrees of freedom during the evolution of the composite system towards a fully equilibrated compound nucleus. Measurement of the evaporation residue cross section in reaction systems with comparatively higher entrance channel mass asymmetry can help further understanding of this aspect.

IV. CONCLUSIONS

In summary, the mass distribution and mass-resolved angular distribution have been measured in the $^{16}O + ^{238}U$ reaction at sub-barrier energy to investigate the dominant NCN fission process. The measurements were carried out by the recoil catcher technique followed by offline γ-ray spectrometry. The mass distribution was observed to be predominantly asymmetric, though small contribution from symmetric fission was also present. Measurement of the mass-resolved angular distribution of fission products showed that the anisotropy values are independent of the fission product mass or asymmetry of mass division, indicating quasifission to be the dominant NCN fission process at sub-barrier energy. This observation is different from that at above-barrier energies in $^{16}O + ^{232}Th$ [16,17], $^{20}Ne + ^{232}Th$ [18], and $^{28}Si + ^{232}Th$ [19] reactions where a systematic increase was observed with decreasing mass asymmetry, which could be explained after including the contribution from preequilibrium fission. In the present work, calculated angular anisotropies were much lower than the experimental values, even after including the contribution from preequilibrium fission, further confirming the fact that the observed anomaly is due to the contribution from quasifission.

ACKNOWLEDGMENT

We thank Dr. Z. Kohley for valuable suggestions.

[1] T. Banerjee *et al.*, Phys. Rev. C **94**, 044607 (2016).
[2] K. Sudarshan, R. Tripathi, S. Sodaye, S. K. Sharma, P. K. Pujari, J. Gehlot, N. Madhavan, S. Nath, G. Mohanto, I. Mukul, A. Jhingan, and I. Mazumdar, Phys. Rev. C **95**, 024604 (2017).
[3] Rafiei *et al.*, Phys. Rev. C **77**, 024606 (2008).
[4] Prasad *et al.*, Phys. Rev. C **81**, 054608 (2010).
[5] Appannababu *et al.*, Phys. Rev. C **83**, 034605 (2011).
[6] P. Shidling, Phys. Lett. B **670**, 99 (2008).
[7] G. Mohonto *et al.*, Nucl. Phys. A **890–891**, 62 (2012).
[8] V. S. Ramamurthy and S. S. Kapoor, Phys. Rev. Lett. **54**, 178 (1985).
[9] V. S. Ramamurthy and S. S. Kapoor, Phys. Rev. C **32**, 2182 (1985).
[10] W. J. Swiatecki, Phys. Scr. **24**, 113 (1981).
[11] R. G. Thomas, R. K. Choudhury, A. K. Mohanty, A. Saxena, and S. S. Kapoor, Phys. Rev. C **67**, 041601(R) (2003).
[12] D. J. Hinde, M. Dasgupta, J. R. Leigh, J. P. Lestone, J. C. Mein, C. R. Morton, J. O. Newton, and H. Timmers, Phys. Rev. Lett. **74**, 1295 (1995).
[13] K. Nishio, H. Ikezoe, Y. Nagame, M. Asai, K. Tsukada, S. Mitsuoka, K. Tsuruta, K. Satou, C. J. Lin, and T. Ohsawa, Phys. Rev. Lett. **93**, 162701 (2004).
[14] K. Banerjee, T. K. Ghosh, S. Bhattacharya, C. Bhattacharya, S. Kundu, T. K. Rana, G. Mukherjee, J. K. Meena, J. Sadhukhan, S. Pal, P. Bhattacharya, K. S. Golda, P. Sugathan, and R. P. Singh, Phys. Rev. C **83**, 024605 (2011).
[15] R. Yanez, D. J. Hinde, B. Bouriquet, and D. Duniec, Phys. Rev. C **71**, 041602(R) (2005).
[16] D. Vorkapic and B. Ivanisevic, Phys. Rev. C **55**, 2711 (1997).
[17] Bency John *et al.*, Phys. Rev. C **51**, 165 (1995).
[18] R. Tripathi, S. Sodaye, K. Sudarshan, and R. Guin, Phys. Rev. C **88**, 024603 (2013).
[19] S. Sodaye, R. Tripathi, B. V. John, K. Ramachandran, and P. K. Pujari, Phys. Rev. C **95**, 014612 (2017).
[20] Trotta *et al.*, Prog. Theor. Phys. Suppl. **154**, 37 (2004).
[21] J. F. Ziegler and J. P. Biersack, TRIM code, version 95.06.
[22] C. H. Dasso and S. Landowne, Comput. Phys. Commun. **46**, 187 (1987).
[23] S. Raman, C. W. Nestor, and P. Tikkanen, A. Data Nucl. Data Tables, **78**, 1 (2001).
[24] R. B. Firestone and V. S. Shirley, *Table of Isotopes*, 8th ed. (Wiley Interscience, New York, 1999).
[25] U. Reus and W. Westmeier, At. Data Nucl. Data Tables **29**, 1 (1983).

[26] P. K. Mukhopadhyay, in *Proceedings of Symposium on Intelligent Nuclear Instrumentation, Mumbai (2001)*, Vol. 33, p. 307; INIS Repository **33**, 33001318 (2001).
[27] S. Sodaye, R. Tripathi, K. Sudarshan, and R. Guin, Phys. Rev. C **87**, 044610 (2013).
[28] E. M. Kozulin, A. Ya. Rusanov, and G. N. Smirenkin, Phys. At. Nucl. **56**, 166 (1993).
[29] S. Kailas *et al.*, Phys. Rev. C **59**, 2580 (1999).
[30] L. J. Colby, Jr., M. L. Shoaf, and J. W. Cobble, Phys. Rev. **121**, 1415 (1961).
[31] R. Leguillon *et al.*, Phys. Lett. B **761**, 125 (2016).
[32] H. H. Rossner, J. R. Huizenga, and W. U. Schröder, Phys. Rev. Lett. **53**, 38 (1984).
[33] R. Vandenbosch and J. R. Huizenga, *Nuclear Fission* (Academic, London, 1973).
[34] I. Halpern and V. M. Strutinsky, in *Proceedings of the Second United Nations International Conference on Peaceful Uses of Atomic Energy, Geneva, 1958*, edited by J. H. Martens *et al.* (United Nations, Geneva, 1958), Vol. 15, p. 408.
[35] H. C. Pauli and T. Ledergerber, Nucl. Phys. A **175**, 544 (1971).
[36] M. Brack, Jens Damgaard, A. S. Jensen, H. C. Pauli, V. M. Strutinsky, and C. Y. Wong, Rev. Mod. Phys. **44**, 320 (1972).
[37] R. W. Hasse and W. D. Myers, *Geometrical Relationships of Macroscopic Nuclear Physics* (Springer-Verlag, Berlin, 1988), pp. 78–82.
[38] T. Datta, S. P. Dange, H. Naik, and S. B. Manohar, Phys. Rev. C **48**, 221 (1993).
[39] M. G. Itkis *et al.*, Yad. Fiz. **53**, 1225 (1991).